Energy-Transfer Mechanisms and Emission Quantum Yields In Eu^{3+}-Based Siloxane-Poly(oxyethylene) Nanohybrids

R. A. Sá Ferreira and L. D. Carlos*

Departamento de Física, Universidade de Aveiro, 3810-193 Aveiro, Portugal

R. R. Gonçalves and S. J. L. Ribeiro

Instituto de Química-UNESP, CP 355, 14801-970 Araraquara SP, Brazil

V. de Zea Bermudez

Departamento de Química, Universidade de Trás-os-Montes e Alto Douro, Quinta de Prados, Apartado 202, 5001-911 Vila Real Codex, Portugal

Received April 5, 2001. Revised Manuscript Received June 28, 2001

We report the energy-transfer mechanisms and emission quantum yield measurements of sol−gel-derived Eu^{3+}-based nanohybrids. The matrix of these materials, classified as diureasils and termed U(2000) and U(600), includes urea cross-links between a siliceous backbone and polyether-based segments of two molecular weights, 2000 and 600, respectively. These materials are full-color emitters in which the Eu^{3+} $^5D_0 \rightarrow {}^7F_{0-4}$ lines merge with the broad green-blue emission of the nanoscopic matrix's backbone. The excitation spectra show the presence of a large broad band (∼27000−29000 cm^{-1}) undoubtedly assigned to a ligand-to-metal charge-transfer state. Emission quantum yields range from 2% to 13.0% depending on the polymer molecular weight and Eu^{3+} concentration. Energy transfer between the hybrid hosts and the cations arises from two different and independent processes: the charge-transfer band and energy transfer from the hybrid's emitting centers. The activation of the latter mechanisms induces a decrease in the emission quantum yields (relative to undoped nanohybrids) and permits a fine-tuning of the emission chromaticity across the Comission Internacionalle d'Éclairage diagram, e.g., (*x*, *y*) color coordinates from (0.21, 0.24) to (0.39, 0.36). Moreover, that activation depends noticeably on the ion local coordination. For the diureasils with longer polymer chains, energy transfer occurs as the Eu^{3+} coordination involves the carbonyl-type oxygen atoms of the urea bridges, which are located near the hybrid's host emitting centers. On the contrary, in the U(600)-based diureasils, the Eu^{3+} ions are coordinated to the polymer chains, and therefore, the distance between the hybrid's emitting centers and the metal ions is large enough to allow efficient energy-transfer mechanisms.

I. Introduction

There is a growing interest in the development of new full-color emitting materials that combine good mechanical, thermal, and chemical stability in air with high room-temperature emission quantum yields.[1−4] Organic/inorganic hybrid materials processed by the sol−gel method are considered to be good candidates to assemble such properties, lending themselves to applications in displays and lighting devices.[4−6] It has been demonstrated that some of the hybrid frameworks recently proposed are luminescent prior to the incorporation of emitting centers (organic dyes and lanthanide ions), a feature that has been poorly explored.[4,7−12] In fact, most of the research has been focused on the

* To whom correspondence should be addressed. E-mail: lcarlos@fis.ua.pt. Phone: 351 234 370946. Fax: 351 234 424965.

(1) Friend, R. H.; Gymer, R. W.; Holmes, A. B.; Burroughes, J. H.; Marks, R. N.; Taliani, C.; Bradley, D. D. C.; Dos Santos, D. A.; Bredas, J. L.; Logdlund, M.; Salaneck, W. R. *Nature* **1999**, *397*, 121.

(2) Cao, Y.; Parker, I. D.; Yu, G.; Zhang, C.; Heeger, A. J. *Nature* **1998**, *397*, 414.

(3) Hide, F.; Diaz-Garcia, M. A.; Schwartz, B. J.; Anderson, M. R.; Pei, Q.; Heeger, A. J. *Science* **1995**, *267*, 1332.

(4) Green, W. H.; Le, K. P.; Grey, J.; Au, T. T.; Sailor, M. J. *Science* **1997,** *276*, 1826.

(5) (a) Sanchez, C.; Ribot, F.; Lebeau, B. *J. Mater. Chem.* **1999**, *9*, 35. (b) Judeinstein, P.; Sanchez, C. *J. Mater. Chem.* **1996**, *6*, 511.

(6) Gomez-Romero, P. *Adv. Mater.* **2001**, *13*, 163.

(7) (a) Carlos, L. D.; de Zea Bermudez, V.; Duarte, M. C.; Silva, M. M.; Silva, C. J.; Smith, M. J.; Assunção, M.; Alcácer, L. In *Physics and Chemistry of Luminescent Materials VI*; Ronda, C., Welker, T., Eds.; Electrochemical Society Proc.: San Francisco, 1998; Vols. 97−29, p 352. (b) de Zea Bermudez, V.; Carlos, L. D.; Duarte, M. C.; Silva, M. M.; Silva, C. J.; Smith, M. J.; Assunção, M.; Alcácer, L. *J. Alloys Compd.* **1998**, *275−277*, 21.

(8) (a) Bekiari, V.; Lianos, P. *Langmuir* **1998**, *14*, 3459. (b) Bekiari, V.; Lianos, P. *Chem. Mater.* **1998**, *10*, 3777.

(9) (a) Carlos, L. D.; de Zea Bermudez, V.; Ferreira, R. A. Sá; Marques, L.; Assunção, M. *Chem. Mater.* **1999,** *11*, 581. (b) de Zea Bermudez, V.; Carlos, L. D.; Alcácer, L. *Chem. Mater.* **1999**, *11*, 569.

(10) (a) Sá Ferreira, R. A.; Carlos, L. D.; de Zea Bermudez, V. *Thin Solid Films* **1999**, *343*, 476. (b) Carlos, L. D.; Sá Ferreira, R. A.; Orion, I.; de Zea Bermudez, V.; Rocha, J. *J. Lumin.* **2000**, *87−89*, 702.

10.1021/cm010311o CCC: $20.00
Published on Web 09/17/2001

photoluminescence features of lanthanide-based hybrid matrixes,[7b,13−23] seeking essentially to take advantage of the high chromaticity and long-lived excited-states characteristic of the metal ions.

The main interest of the organic/inorganic hybrid concept basically derives from the possibility of tailoring the properties of novel multifunctional advanced materials through the combination at the nanosize level of the organic and inorganic components in a single material.[5,6] This is, for instance, well illustrated by the series of recent reports on multifunctional host nanohybrids, termed diureasils, based on a siloxane backbone covalently bonded to poly(oxyethylene), POE, chains (of variable molecular weight) by means of urea cross-links.[7,9−13,19−22] The emission of the diureasils presents a blue component originated from electron−hole recombinations in the NH groups of the urea linkages and a purple-blue one assigned to electron−hole recombinations occurring in the siliceous nanodomains.[9a,10,12] The energy of this latter emission strongly depends on the excitation wavelength,[9a,10] making the tunability of the host emission color across the Comission Internacionalle d'Éclairage, CIE, diagram possible.[10b] The variation of the polymer chain length also results in a shift of the energetic spectral emitting region, thus allowing again the color emission to be tuned.[10b]

Upon the incorporation of lanthanide ions in the diureasil host, namely, Eu^{3+},[7,13,19−21] Tb^{3+},[17] and Nd^{3+},[22] the luminescence spectrum is substantially altered, showing the intrinsic hybrid's broad band emission superposed on the characteristic intra-4f sharp lines. Moreover, the energy and relative intensity of the backbone luminescence with respect to the Eu^{3+} lines depend on the lanthanide concentration and therefore on the ion local coordination.[19,20] For instance, the nature of the Eu^{3+} first coordination shell in these nanocomposites varies both with the salt concentration and with the polymer molecular weight.[19,20] In the diureasils containing long organic segments, the Eu^{3+} ions interact mainly with the carbonyl-type oxygen atoms of the urea cross-links, located at the organic−inorganic interface, as long as the saturation of these groups is not attained. On the contrary, in the diureasils with shorter polymer chains, the lanthanide ions are unable to disrupt the characteristic strong and ordered hydrogen-bonded urea−urea structures, and therefore, the preferential coordination sites are the ether oxygen atoms of the polymer chains.[20] However, at high salt concentration, besides the coordination to the polymer ether oxygen atoms, a distinct cation local site environment involving the interaction with the urea carbonyl oxygen atoms at the siloxane−POE interface is detected.[20]

In these nanocomposites energy-transfer mechanisms between the hybrid host and the metallic ions have not been studied yet, despite their potential relevant implications for the observed overall emission features. In fact, even for other classes of polymer-based materials modified by lanthanide salts, this subject has been discussed in few reports. We can emphasize, for instance, the study of the energy-transfer mechanisms from semiconducting blue-emitting conjugated polymers to Eu^{3+} β-diketonate complexes.[23a]

In lanthanide coordination compounds the so-called *antenna effect* (i.e., absorption of ultraviolet light by the ligand cage-type hosts, intramolecular energy transfer to the luminescent center, and subsequent enhanced emission) is the base of efficient ultraviolet/visible (UV/vis) conversion.[24] In addition, ligand-to-metal charge-transfer (LMCT) states may also appear due to the active ion−first ligand interactions. These states usually play the role of nonradiative channels, contributing to depopulate the ion excited sates at room temperature.[25−28] An unequivocal assignment and detection of these LMCT states have been performed only in a few lanthanide compounds, due to the general difficulty in detecting these states by absorption and emission spectroscopy.[24b,28]

In the present work we aim at gaining a deeper understanding of the Eu^{3+}-based diureasil emission properties. The existence of energy transfer between the hybrid hosts and the lanthanide ions is clearly demonstrated using essentially experimental emission quantum yields and photoluminescence excitation spectroscopy. The influence of the cation local coordination on this energy-transfer process is also discussed. Finally, solid arguments that corroborate our earlier assumption[19a] indicating the presence of LMCT sates in the Eu^{3+}-based diureasils are presented.

II. Experimental Section

Synthesis. The sol−gel-derived organic/inorganic nanohybrids investigated in this work were synthesized using a procedure already described.[7,19] The sol−gel reaction can be

(11) Bekiari, V.; Lianos, P.; Stangar, U. L.; Orel, B.; Judeinstein, P. *Chem. Mater.* **2000**, *12*, 3095.
(12) Carlos, L. D.; Sá Ferreira, R. A.; de Zea Bermudez, V.; Ribeiro, S. J. L. *Adv. Funct. Mater.* **2001**, *2*, 111.
(13) Ribeiro, S. J. L.; Dahmouche, K.; Ribeiro, C. A.; Santilli, C. V.; Pulcinelli, S. H. J. *J. Sol-Gel Sci. Technol.* **1998**, *13*, 427.
(14) (a) Matthews, L. R.; Knobbe, E. T. *Chem. Mater.* **1993**, *5*, 1697. (b) Costa, V. C.; Lochhead, M. J.; Bray, K. L. *Chem. Mater.* **1996**, *8*, 783.
(15) (a) Franville, A. C.; Zambon, D.; Mahiou, R. *Chem. Mater.* **2000**, *12*, 428. (b) Franville, A. C.; Zambon, D.; Mahiou, R.; Chou, S.; Troin, Y.; Cousseins, J. C. *J. Alloys Compd.* **1998**, *275−277*, 831.
(16) (a) Li, H.-H.; Inoue, S.; Ueda, D.; Machida, K.-I.; Adachi, G.-Y. *Electrochem. Solid-State Lett.* **1999**, *2*, 354. (b) Li, H.-H.; Inoue, S.; Machida, K.-I.; Adachi, G.-Y. *Chem. Mater.* **1999**, *11*, 3171.
(17) Bekiari, V.; Lianos, P.; Judeinstein, P. *Chem. Phys. Lett.* **1999**, *307*, 310.
(18) Tanner, P. A.; Yan, B.; Zhang, H. *J. Mater. Sci.* **2000**, *35*, 4325.
(19) (a) Carlos, L. D.; Sá Ferreira, R. A.; de Zea Bermudez, V.; Molina, C.; Bueno, L. A.; Ribeiro, S. J. L. *Phys. Rev. B* **1999**, *60*, 10042. (b) Carlos, L. D.; Messaddeq, Y.; Brito, H. F.; Sá Ferreira, R. A.; de Zea Bermudez, V.; Ribeiro, S. J. L. *Adv. Mater.* **2000**, *12*, 594.
(20) de Zea Bermudez, V.; Sá Ferreira, R. A.; Carlos, L. D.; Molina, C.; Dahmouche, K.; Ribeiro, S. J. L. *J. Phys. Chem. B* **2001**, *105*, 3378.
(21) Silva, M. M.; de Zea Bermudez, V.; Carlos, L. D.; Almeida, A. P.; Smith, M. J. *J. Mater. Chem.* **1999**, *9*, 1735.
(22) Carlos, L. D.; Sá Ferreira, R. A.; de Zea Bermudez, V. *Electrochim. Acta* **2000**, *45*, 1467.
(23) (a) McGhee, M. D.; Bergstedt, T.; Zhang, C.; Saab, A. P.; O'Regan, M. B.; Bazan, G. C.; Srdanov, V. I.; Heeger, A. J. *Adv. Mater.* **1999**, *11*, 1349. (b) Isakawi, M.; Kuraki, J.; Ito, S. *J. Sol-Gel Sci. Technol.* **1998**, *13*, 587.
(24) (a) Sabbatini, N.; Guardigli, M.; Lehn, J.-M. *Coord. Chem. Rev.* **1993**, *123*, 201. (b) De Sá, G. F.; Malta, O. L.; De Mello Donegá, C.; Simas, A. M.; Longo, R. L.; Santa-Cruz, P. A.; Silva, E. F., Jr. *Coord. Chem. Rev.* **2000**, *196*, 165.
(25) (a) Struck, C. W.; Fonger, W. H. *J. Lumin.* **1970**, *1*, 456. (b) Struck, C. W.; Fonger, W. H. *J. Chem. Phys.* **1970**, *52*, 6364.
(26) Blasse, G.; Sabatini, N. *Mater. Chem. Phys.* **1987**, *16*, 237.
(27) Struck, C. W.; Fonger, W. H. *Understanding Luminescence Spectra and Efficiency Using Wp and Related Functions*; Springer-Verlag: Berlin, 1978.
(28) De Mello Donegá, C.; Ribeiro, S. J. L.; Gonçalves, R. R.; Blasse, G. *J. Phys. Chem. Solids* **1996**, *57*, 1727.

summarized in two main steps. Step 1 corresponds to the formation of urea linkages between the terminal amine groups of two double functional diamines (commercially designated as Jeffamine ED-2001 and Jeffamine ED-600, Fluka) and the isocyanate group of an alkoxysilane precursor (3-isocyanatopropyltriethoxysilane, ICPTES, Fluka). This step leads to the formation of the nonhydrolyzed precursor hybrids. In the second stage, the addition of a mixture of water and ethanol leads to hydrolysis and condensation reactions, transforming the precursor into the final xerogels. The structure is represented at the top of Figure 1.

Europium and gadolinium trifluoromethanesulfonate (Aldrich), $Eu(CF_3SO_3)_3$ and $Gd(CF_3SO_3)_3$, were incorporated in this second step, by dissolving them in the water and ethanol mixture (molar ratio 1 ICPTES:4 CH_3CH_2OH:1.5 H_2O). The doped nanohybrids have been designated as $U(Y)_nLn(CF_3SO_3)_3$ (Ln = Eu, Gd), where Y is related to the Jeffamine molecular weight (600 and 2000, respectively; 8.5 and 40.5 polymer repeat units, respectively) and n = [O]/[Eu] represents the number of ether-type oxygen atoms of PEO per Ln^{3+} cation. $U(600)_nEu(CF_3SO_3)_3$ and $U(2000)_nEu(CF_3SO_3)_3$ were synthesized with $20 \leq n \leq 200$ and $40 \leq n \leq 400$, respectively, corresponding to a variation of the Eu^{3+} content versus the total mass between 4.79% and 0.58% for $U(600)_nEu(CF_3SO_3)_3$ and between 4.96% and 0.60% for $U(2000)_nEu(CF_3SO_3)_3$. Two $U(Y)_{80}Gd(CF_3SO_3)_3$, Y = 2000 and 600, diureasils were prepared.

Methods. Room-temperature emission, excitation, and diffuse reflectance spectra were recorded under a 450 W Xe arc lamp excitation with a SPEX Fluorolog F212I spectrofluorimeter coupled to a Hamamatsu R928 photomultiplier. All the spectra were corrected for optics and detection spectral response.

The absolute emission quantum yield, ϕ, was measured at room temperature by the experimental technique described by Wrighton et al.,[29] and it was calculated by the following expression:

$$\phi = A/(R_S - R_H) \quad (1)$$

where A is the area under the hybrid's emission spectra, and R_S and R_H are the diffuse reflectances, with respect to a fixed wavelength, of the diureasils and of the reflecting standard, respectively. As a standard we used KBr, previously stored in an oven at 353 K. In the experimental method, the powder size and packing fraction are crucial factors, since the R_S and R_H intensities depend on them. Taking this point into account, the diffuse reflectance was first measured at a wavelength not absorbed by the nanohybrids. The diureasils were thoroughly ground until R_H totally overlapped R_S, indicating similar powder sizes and packing fractions. Diffuse reflectance and emission spectra were detected at a 24.5° angle, relative to the incident light. The same experimental conditions were fixed for all the measurements. The errors in the quantum yields associated with this technique are estimated within 10%.[30]

III. Results and Discussion

Excitation Spectra. Figure 1 shows the excitation spectra for the $U(600)_{200}Eu(CF_3SO_3)_3$ diureasil monitored along the hybrid's backbone emission. A broad band is observed in the region between 300 and 500 nm. As the detection wavelength increases, the spectrum maximum intensity shifts to lower energies and the broad band full width at half-maximum (fwhm) increases from 3000 to 6000 cm^{-1}. Moreover, for detection wavelengths higher than 435 nm, another band centered at ~420 nm (marked with an asterisk in Figure 1) is detected. Its relative intensity with respect to the excitation maximum intensity increases with the increase of the monitored wavelength. The energy of this band does not depend on the detection wavelength, contrary to the more intense one for which a linear relation between the maximum intensity position and the respective detection energy is observed (inset of Figure 1). This behavior is maintained until the detection wavelength reaches ~610−615 nm, as we will show later.

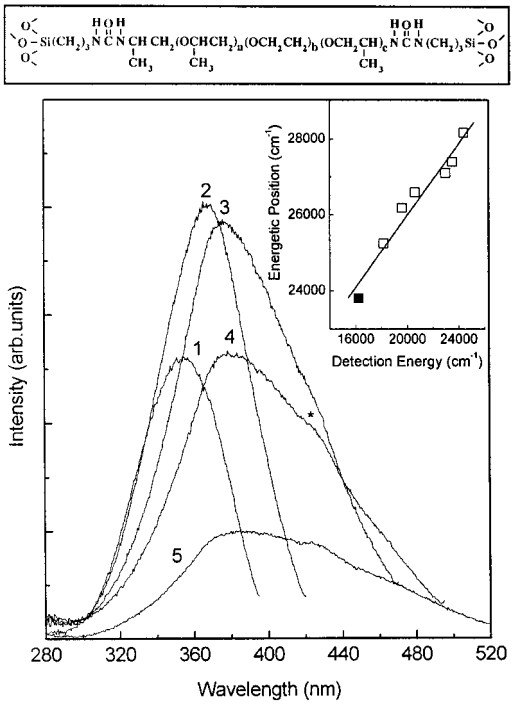

Figure 1. Undoped deureasil structure, $a + c = 2.5$ and $b = 8.5$ and 40.5 for U(600) and U(2000), respectively (top). Excitation spectra for the $U(600)_{200}Eu(CF_3SO_3)_3$ diureasil monitored at (1) 410, (2) 435, (3) 485, (4) 510, and (5) 550 nm. The inset shows the excitation spectra maximum intensity position versus the respective detection energy along the hybrid's emission band for $U(600)_{200}Eu(CF_3SO_3)_3$. The solid square represents the excitation of the hybrid backbone detected at the strongest $^7F_2$ line, 616 nm. The solid line corresponds to the data linear fit.

The previous results establish the presence of two emitting centers, similarly to what we have already observed and reported for the undoped hosts.[9a,10,12] In the U(2000) and U(600) hosts, the respective 14 K excitation spectra display a large broad band between 315 and 450 nm, where two components were also clearly distinguished.[9a,10] The less energetic band and the more energetic one were assigned to the preferential excitation of the NH groups and siliceous domains, respectively.[9a,10,12] Likewise to what we have reported for the undoped hosts,[9a,12] the dependence of the more energetic excitation peak on the detection wavelength, contrary to what is observed for the 420 nm band (Figure 1), corroborates the above attribution.

The excitation spectra monitored at the strongest $^5D_0 \rightarrow {}^7F_2$ Eu^{3+} emission line, for $U(600)_nEu(CF_3SO_3)_3$, $20 \leq n \leq 200$, and for $U(2000)_nEu(CF_3SO_3)_3$, $40 \leq n \leq 400$, are plotted in parts a and b, respectively, of Figure 2. The main large broad band, centered at ~340 and ~365 nm for the diureasils with shorter and longer polymer

(29) Wrighton, M. S.; Gingley, D. S.; Morse, D. L. *J. Phys. Chem.* **1974**, *78*, 2229.
(30) Bril, A.; De Jager-Veenis, A. W. *J. Res. Nat. Bur. Stand.* **1976**, *80A*, 401.

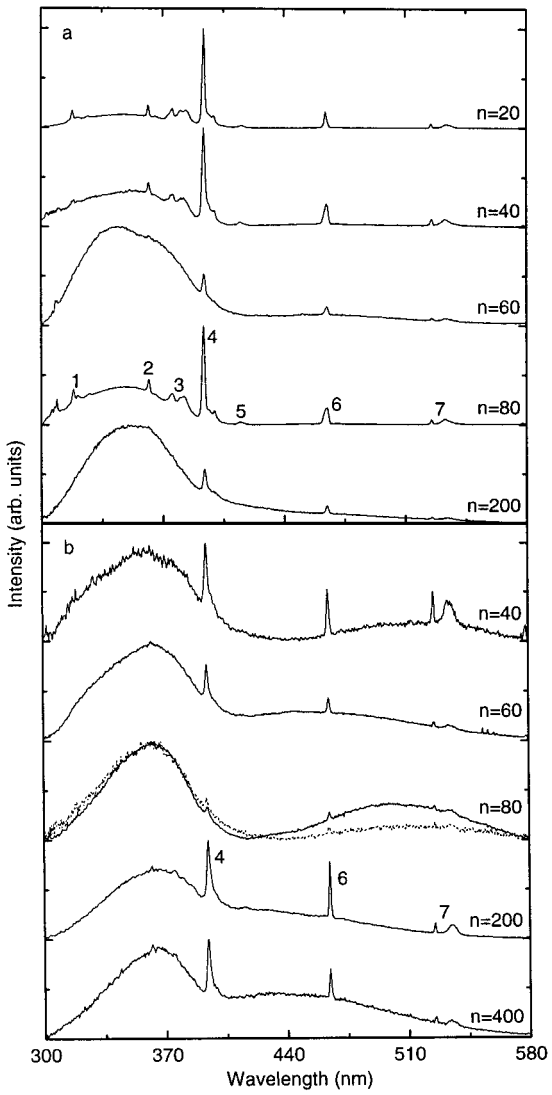

Figure 2. Excitation spectra for (a) $U(600)_nEu(CF_3SO_3)_3$ and (b) $U(2000)_nEu(CF_3SO_3)_3$. Overlapping the $U(2000)_{80}Eu(CF_3SO_3)_3$ excitation spectra is plotted the respective spectrum detected at 700 nm (dashed line). (1), (2), (3), (4), (5), (6), and (7) correspond to $^7F_0 \rightarrow {}^5H_4$, $^5D_4$, ^5G_J, $^5L_6$, $^5D_3$, $^5D_2$, and $^5D_1$.

chains, respectively, was already observed at 14 K in the latter nanohybrids and was ascribed to a LMCT transition resulting from the interaction between the ion and the first ligands.[19a] At higher wavelengths, 420−540 nm, a second broad band is also detected. These two bands overlap a series of sharp lines assigned to intra-$4f^6$ transitions between the $^7F_0$ and the $^5H_4$, ^5G_J, $^5L_6$, and $^5D_{3-1}$ levels.

The band detected at higher wavelengths, although present in the $U(600)_nEu(CF_3SO_3)_3$ diureasils, has a greater contribution to the $U(2000)_nEu(CF_3SO_3)_3$ spectra. Its respective maximum intensity position follows the linear relation found for the excitation spectra monitored along the hybrid's emission (inset of Figure 1) within the respective europium concentration. On the contrary, the energy of the LMCT band is blue-shifted relative to the hybrid's backbone excitation spectra. To verify whether the nature of this band is also related to charge-transfer processes, two experiments were done: (i) another Eu^{3+} transition was monitored, the $^5D_0 \rightarrow {}^7F_4$ line at 700 nm, (ii) the excitation spectra of the Gd^{3+}-based nanohybrids were recorded under the same previous experimental conditions used for the diureasils modified by $Eu(CF_3SO_3)_3$. The Gd^{3+} excitation spectrum is a useful tool, since the energetic difference between the first excited state and the fundamental levels is too high to allow the detection of a charge-transfer state in the UV/vis range. By doing this, we expect to measure in the Gd^{3+} excitation spectra only the contributions that are not related to the charge-transfer processes. The excitation spectrum monitored at 700 nm is plotted in Figure 2b for $U(2000)_{80}Eu(CF_3SO_3)_3$, together with the one detected at 616 nm, for an easier comparison. No changes are observed in the energy and fwhm of the LMCT band. In addition, the intensity of the band observed at longer wavelengths is approximately half-reduced. For both Gd^{3+}-based diureasil series, the presence of the LMCT states was not detected and only the less intense band could be discerned. These results clearly assigned this band to excitation levels of the hybrid nanoscopic matrix. First, the detection of this band in the Gd^{3+} excitation spectra immediately excludes any connection with charge-transfer mechanisms. Second, the observed decrease in its intensity, with respect to the LMCT band, should not happen if both bands have the same origin. The emission spectra (see the next section) corroborate the above assignment of that band to the hybrid's emitting centers. As the emission of these centers overlaps the Eu^{3+} luminescence (Figure 3a), emission arising from the diureasil backbone is detected, when the Eu^{3+} lines are monitored.

The $U(600)_nEu(CF_3SO_3)_3$ nanohybrids always present a LMCT band at higher energy than those displayed by the $U(2000)_nEu(CF_3SO_3)_3$ hybrids, for the whole concentration range studied here. It is known that a shift of the LMCT transition frequencies toward the high-energy region of the spectrum is related to an increase of the effective charge of the lanthanide cation and, thus, to a decrease of the tendency of the first-shell ligands to bond covalently to the metal ion.[31] Therefore, this suggests that the Eu^{3+} ions experience a more covalent environment in the $U(2000)_nEu(CF_3SO_3)_3$ samples than in the $U(600)_nEu(CF_3SO_3)_3$ samples. This fact is mainly induced by alterations in the type of ligands present in the first coordination shell.[20] In $U(2000)_nEu(CF_3SO_3)_3$, $40 \leq n \leq 400$, the Eu^{3+} is coordinated to the urea carbonyl oxygen atoms.[19] In $U(600)_nEu(CF_3SO_3)_3$ ether-type oxygen atoms of the polymer surround the ion for $n \geq 40$, and only for higher Eu^{3+} concentrations, $n = 20$, the coordination to the oxygen atoms of the urea groups was observed together with the presence of the Eu^{3+} located in the polymer chains.[20] The oxygen atoms of the carbonyl groups are known to have a greater tendency to bond covalently to the Eu^{3+} ions, when compared with the ether oxygen atoms.[32] In this way, a more energetic LMCT band is expected in the case of the $U(600)_nEu(CF_3SO_3)_3$ diureasils. The number of ligands present in the Eu^{3+} first coordination shell also depends on the concentration of the Eu^{3+} in the nanocomposites, so changes in the energy of the LMCT states by varying the Eu^{3+} content,

(31) Ovsyankin V. V. In *Spectroscopy of Solids Containing Rare Earth Ions*; Kaplyanskii, A. A., MacFarlane, R. M., Eds.; Elsevier Publishers: Amsterdam, 1987; p 371.

(32) Frey, S. T.; Horrocks, W. De W., Jr. *Inorg. Chim. Acta* **1995**, *229*, 383.

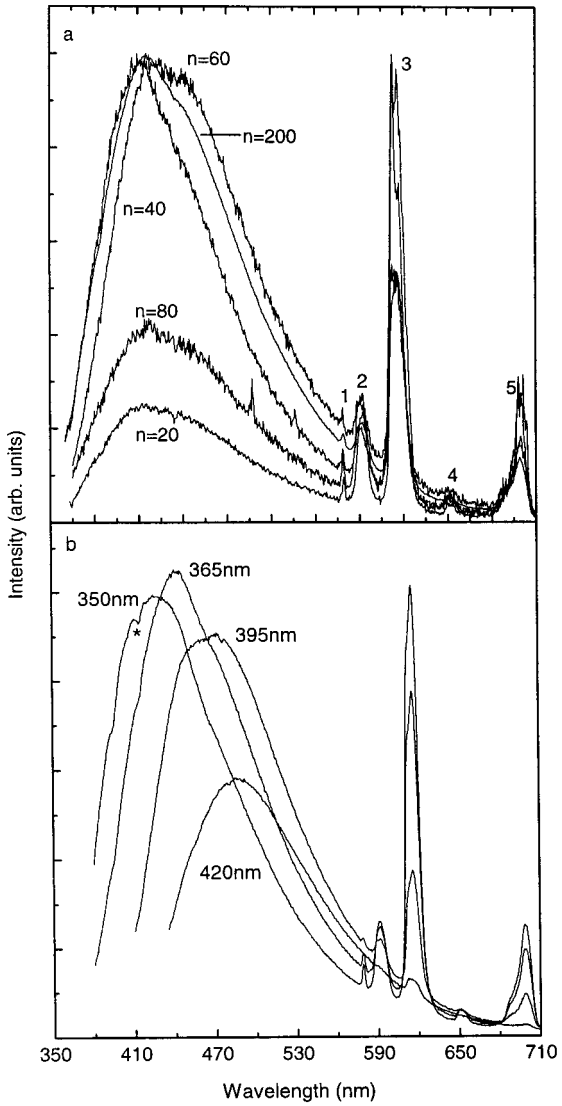

Figure 3. Emission spectra of (a) $U(600)_nEu(CF_3SO_3)_3$ and (b) $U(600)_{200}Eu(CF_3SO_3)_3$ recorded under the excitations mentioned. (1), (2), (3), (4), and (5) correspond to $^5D_0 \rightarrow {}^5F_{0-4}$. The asterisk marks the $^7F_0 \rightarrow {}^5L_6$ self-absorption.

inside each xerogel series, are also expected as one can observe recalling Figure 2. For the $U(600)_nEu(CF_3SO_3)_3$ xerogels the energy of the LMCT states is always centered at ~340 nm, indicating that possible changes in the first neighbor number, for $40 \leq n \leq 200$, or the presence of another ion local coordination site, for $n \leq 20$, does not seem to affect significantly the covalency degree of the first coordination shell. However, the doped nanohybrids with longer polymer chains show a displacement in the energy of the LMCT band ascribed to variations in the chemical nature of the first neighbors.[19a]

Emission Spectra. Figure 3a presents the emission spectra for the entire series of $U(600)_nEu(CF_3SO_3)_3$ diureasils, excited at 375 nm. The spectra are composed of a large broad band in the green-blue spectral region, already observed in the undoped nanohybrids,[7,9−12] that overlaps a series of Eu^{3+} intra-$4f^6$ yellow-red sharp lines, assigned to transitions between the $^5D_0$ and the $^7F_{0-4}$ levels. The large broad band results from the overlap of two distinct emissions assigned to electron−hole recombinations in the NH groups of the urea bridges and in the siliceous domains of the inorganic backbone.[12] The maximum intensity energetic position of the broad band and its relative intensity with respect to the cation lines strongly depend on the amount of Eu^{3+} incorporated, Figure 3a. For $U(600)_nEu(CF_3SO_3)_3$, the larger overlap between the hybrid's backbone emission and the Eu^{3+} lines is detected for $n = 200$ and 60, in agreement with the increase of the hybrid backbone intensity observed in the excitation spectra monitored around the Eu^{3+} lines (Figure 2a). A red shift of the maximum intensity energetic position with the increase of the excitation wavelength is observed, exemplified in Figure 3b for $U(600)_{200}Eu(CF_3SO_3)_3$.

The emission of the $U(600)_nEu(CF_3SO_3)_3$ diureasils appears to be white to the naked eyes, as shown in the CIE (x, y) chromaticity diagram of Figure 4a for two typical samples, $n = 20$ and 200. The color coordinates of the remaining compositions are very similar to the ones of $U(600)_{200}Eu(CF_3SO_3)_3$. The ability to tune the hybrid's emission to colors across the chromaticity diagram is readily achieved by changing either the amount of Eu^{3+} incorporated in the diureasil host and/or the excitation wavelength, Figure 4a. The $U(2000)_nEu(CF_3SO_3)_3$ emission spectra are also composed of the convolution of the hybrid's and Eu^{3+} emission, presenting the same luminescence properties mentioned above for the $U(600)_nEu(CF_3SO_3)_3$ diureasils, despite a red shift of the hybrid's backbone emission.[19] As the energy of the Eu^{3+} emission lines and their relative intensity, with respect to the host emission, depend on the polymer molecular weight, the emission color of the diureasils can also be fine controlled by altering the molecular weight of the polymer chains. For instance, the (x, y) color coordinates of the two $U(Y)_{40}Eu(CF_3SO_3)_3$ nanocomposites, excitation wavelength of 395 nm, are (0.23, 0.23) and (0.39, 0.36), for $Y = 600$ and 2000, respectively (Figure 4b).

Absolute Emission Quantum Yield Measurements and Quantum Efficiency of the $^5D_0$ State. The emission quantum yields were measured for several excitation wavelengths corresponding to (i) the maximum intensity of the hybrid's backbone excitation spectra, (ii) around the maximum intensity of the LMCT band, and (iii) three wavelengths related to direct excitation of Eu^{3+} levels, namely, 395 nm ($^5L_6$), 420 nm ($^5D_3$), and 465 nm ($^5D_2$). Figure 5a presents the values obtained for $U(Y)_{200}Eu(CF_3SO_3)_3$, $Y = 600$ and 2000 (and respective errors bars), as a function of the excitation wavelength. For both diureasil series, and independently of the Eu^{3+} concentration, ϕ presents the same trend; that is, when the excitation wavelength varies between 340 and 500 nm, a maximum value is measured around 395 nm. This wavelength maximizes the emission quantum yields because it corresponds to the greater overlap between the excitation spectra of the two hybrid's emitting centers (see Figure 1). In the doped U(2000) samples ϕ undergoes a decrease from 13.0%, $n = 400$, to 1.4%, $n = 40$. In these nanohybrids, excluding $n = 400$, lower quantum yield values were measured, when compared to the undoped nanocomposite that presents $\phi \approx 9.0\%$.[12] The quantum yield values for $U(600)_nEu(CF_3SO_3)_3$, $n \geq 40$, are similar to the one found for the undoped host, 7.0%,[12] within the experimental error. However, the more concentrated

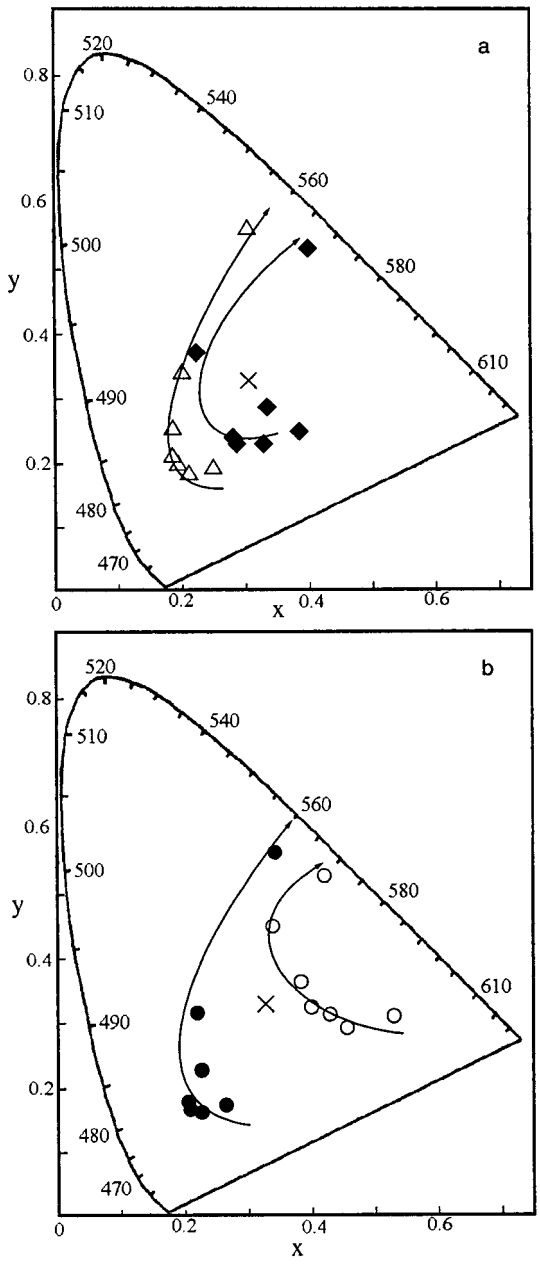

Figure 4. CIE chromaticity diagram showing the (*x*, *y*) color coordinates (calculated for the 2° standard observer) for (a) $U(600)_nEu(CF_3SO_3)_3$, $n = 20$ (open triangles), 200 (solid diamonds), and (b) $U(Y)_{40}Eu(CF_3SO_3)_3$, $Y = 2000$, 600, open and solid circles, respectively. The lines through the data are drawn as guides to the eyes indicating changes in the (*x*, *y*) coordinates as the excitation wavelength increases from 330 to 465 nm. The equienergy white point (0.33, 0.33) is marked with a times sign.

sample, $n = 20$, presents a lower value, $\phi \approx 2.6\%$. All these results (obtained at a 395 nm excitation wavelength) are shown in Figure 5b. There are few results concerning the determination of the absolute quantum yields in lanthanide-based organic/inorganic materials.[23] The diureasil's quantum yields, although smaller than those reported for semiconducting conjugated polymers doped with Eu^{3+} β-diketonate complexes, 17−27%,[23a] are similar to those of the Ce^{3+}-based organic/inorganic hybrids, 4.6−11%.[23b]

The decrease in the emission quantum yields observed for both nanohybrid series as the Eu^{3+} amount incorporated in the diureasil host increases (Figure 5b) is a

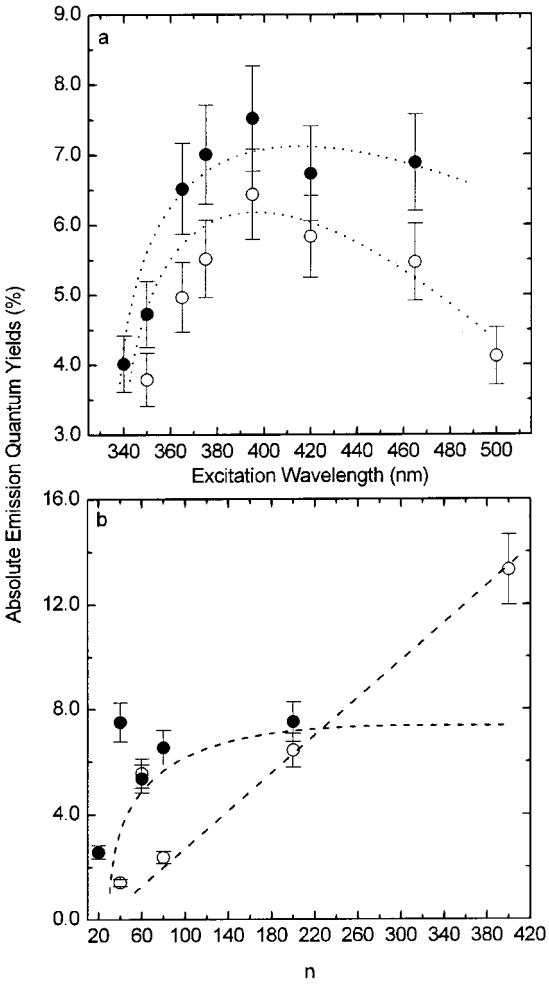

Figure 5. ϕ values for (a) $U(2000)_{200}Eu(CF_3SO_3)_3$ (open circles) and $U(600)_{200}Eu(CF_3SO_3)_3$ (solid circles), excitation wavelengths between 340 and 500 nm, and (b) $U(2000)_nEu(CF_3SO_3)_3$ (open circles) and $U(600)_nEu(CF_3SO_3)_3$ (solid circles). Lines are drawn as guides to the eyes.

clear evidence of energy transfer between the emitting centers of the matrix (donors) and the metal ions (acceptors).[33] Moreover, the results obtained for the emission quantum yields demonstrate that the energy-transfer processes strongly depend of the Eu^{3+} local coordination. In the $U(2000)_nEu(CF_3SO_3)_3$ diureasils as the Eu^{3+} ions interact mainly with the carbonyl-type oxygen atoms of the urea cross-links, located near the hybrid's emitting centers, the energy-transfer processes are active, except in the less concentrated sample, $n = 400$. As the ion concentration increases from $n = 200$ to $n = 40$, more ions are located near the hybrid's emitting centers, which means that there are a higher number of emitting centers transferring energy to the Eu^{3+}, thus contributing to a continuous decrease of the emission quantum yields. On the contrary, in the $U(600)_nEu(CF_3SO_3)_3$, $40 \leq n \leq 200$, nanohybrids, the Eu^{3+} ions are coordinated to the ether oxygen atoms of the polymer chains and the distance between the hybrid's emitting centers and the metal ions is large enough to allow efficient energy transfer. However, for high salt concentration, $n \leq 20$, a distinct cation local

(33) Reisfeld, R.; Jørgenson, C. K. In *Handbook on the Physics and Chemistry of Rare Earths*; Gschneider, K. A., Jr., Eyring L., Eds.; Elsevier Science Publishers: Amsterdam, 1987; Vol. 9, p 61.

site environment involving the interaction with the urea carbonyl oxygen atoms is detected, besides the coordination to the polymer ether oxygen atoms. Therefore, the energy-transfer processes between the hybrid's backbone and the Eu^{3+} ions are activated with the corresponding decrease of the absolute emission quantum yield (Figure 5b). The control of the energy-transfer mechanism activation by changing the ion coordination local site, that is, by changing the polymer molecular weight and/or the Eu^{3+} concentration, allows a fine-tuning of the chromaticity of the diureasil emission. For instance, comparing a sample where the energy-transfer mechanisms are inactive, $U(600)_{40}Eu(CF_3SO_3)_3$, with other nanohybrids where those processes are very efficient, $U(2000)_{40}Eu(CF_3SO_3)_3$, we observe that the ($x$, y) color coordinates of the latter diureasil are shifted to the red region of the CIE diagram, Figure 4b. This is a direct consequence of a decrease in the blue-green hybrid host emission, with respect to the yellow-red intra-$4f^6$ lines, due the activation of the energy-transfer mechanisms discussed above.

All the presented emission quantum yield results are related to the global white light emission that corresponds to the overlap of the hybrid's and ion emission. This is justified since the Eu^{3+} contribution to the global white light emission is small, when compared with the large emission band of the hybrid's backbone. However, we can estimate the efficiency, q, of the $^5D_0$ Eu^{3+} excited state. Assuming that only nonradiative and radiative processes are essentially involved in the depopulation of the $^5D_0$ state, q can be defined as

$$q = \frac{k_r}{k_r + k_{nr}} \tag{2}$$

where k_r and k_{nr} are the radiative and nonradiative probabilities, respectively. The emission intensity, I, taken as the integrated intensity of the $^5D_0 \rightarrow {}^7F_{0-4}$ emission lines can be expressed by

$$I_{i\rightarrow j} = \hbar w_{i\rightarrow j} A_{i\rightarrow j} N_i \tag{3}$$

where i and j represent the initial ($^5D_0$) and final ($^7F_{0-4}$) levels, respectively, $\hbar w_{i\rightarrow j}$ is the transition energy, $A_{i\rightarrow j}$ corresponds to Einstein's coefficient of spontaneous emission, and N_i is the population of the $^5D_0$ emitting level. The radiative contribution, k_r, may be calculated from the relative intensities of the $^5D_0 \rightarrow {}^7F_{0-4}$ lines. Since the $^5D_0 \rightarrow {}^7F_1$ transition can be considered as a reference, due to its dipolar magnetic nature, k_r can be calculated as

$$k_r = \frac{A_{0-1}E_{0-1}}{S_{0-1}} \sum_{J=0}^{4} \frac{S_{0-J}}{E_{0-J}} \tag{4}$$

where A_{0-1} is Einstein's coefficient of spontaneous emission between the $^5D_0$ and the $^7F_1$ levels, which is usually referenced as equal to 50 s^{-1},[34] and E_{0-J} and S_{0-J} are the energy and the integrated intensity of the $^5D_0 \rightarrow {}^7F_J$ transition, respectively. The parameter k_{nr} can be calculated by the $^5D_0$ experimental decay time, τ_{exp}, considering that $(\tau_{exp})^{-1} = k_r + k_{nr}$.

(34) Hazenkamp, M. F.; Blasse, G. *Chem. Mater.* **1990**, *2*, 105.

These results have already been reported for the $U(2000)_nEu(CF_3SO_3)_3$ nanocomposites, $40 \leq n \leq 400$.[19b] In the case of $U(600)_nEu(CF_3SO_3)_3$, we restricted our calculations to the nanohybrids with $n \geq 40$ because for higher salt concentrations two Eu^{3+} different coordination sites are observed and we cannot individualize the two contributions, both in the emission spectra and in the experimental decay. We found quantum efficiency values, $q \approx 13\%$, similar to the ones calculated for the diureasil series with longer polymer chains, in the same concentration range.[19b]

By analyzing the relative energy of the LMCT states between the $U(2000)_nEu(CF_3SO_3)_3$ and the $U(600)_nEu(CF_3SO_3)_3$ nanohybrids, we could expect a greater q value for the latter system, since it is known that lower-lying charge-transfer states contribute in a more efficient way to the nonradiative depopulation of the $^5D_0$ level.[28] Generally, high q values (80−90%) are only found in the case of LMCT positions above 40000 cm^{-1}. Since we are in the presence of LMCT states positioned at considerably lower energies (27000−29000 cm^{-1}), an important overlap with the ion levels clearly contributes to the effective depopulation of the $^5D_0$ level in the diureasils.

Energy Transfer between the Emitting Centers of the Nanoscopic Matrix and the Eu^{3+} Ions. The efficiency of the energy transfer, η, between two species—the donor and the acceptor—can be evaluated by measuring the absolute emission quantum yield in the presence, ϕ, and absence, ϕ_0, of the acceptor[33]

$$\eta = 1 - \frac{\phi}{\phi_0} \tag{5}$$

We estimate the efficiency of the energy transfer for all the nanohybrids of both series where a decrease in the quantum yield value was observed, with respect to the value measured for the corresponding undoped xerogel. Thus, whereas for the $U(2000)_nEu(CF_3SO_3)_3$ series the $n = 400$ sample is the only one where energy-transfer processes seem to be unimportant (as clearly expressed by the increase of the emission quantum yield, with respect to the undoped host), for the $U(600)_nEu(CF_3SO_3)_3$ nanohybrids the energy-transfer mechanisms are activated only for $n = 20$ (Figure 5b). In $U(2000)_nEu(CF_3SO_3)_3$ the efficiency of the energy transfer ranges from 27%, $n = 200$, to 84%, $n = 40$. The value found in $U(600)_{20}Eu(CF_3SO_3)_3$ is 63%. These results, calculated for an excitation wavelength of 395 nm, are independent of the excitation wavelength.

Parts a and b of Figure 6 show a schematic illustration of the LMCT states, hybrid's host emitting centers, and Eu^{3+} levels for $U(2000)_nEu(CF_3SO_3)_3$ and $U(600)_nEu(CF_3SO_3)_3$, respectively. For the LMCT band and the hybrid's host emitting levels the diagram depicts the lower and the higher energy limits obtained for the different excitation wavelengths (300−420 nm) and for the Eu^{3+} content where energy transfer between the host and the cations occurs. We notice that the energy range of the emitting siliceous nanodomains represented in Figure 6 depends on the Eu^{3+} concentration incorporated in the diureasil matrix in such a way that an increase in the siliceous network dimension results in a decrease of the corresponding energy gap.[9,21] Accordingly, Figure 7 illustrates for $U(2000)_nEu(CF_3SO_3)_3$, 40

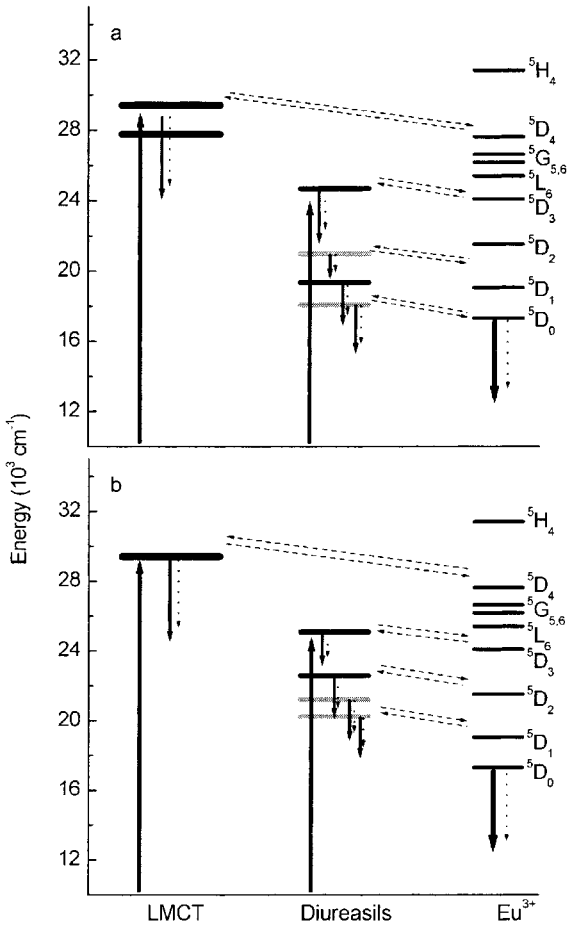

Figure 6. Schematic illustration of the energy diagram for (a) $U(2000)_nEu(CF_3SO_3)_3$, $40 \leq n \leq 200$, and (b) $U(600)_{20}Eu(CF_3SO_3)_3$. For the hybrid's levels the black and gray lines correspond to the siliceous and NH group emitting centers, respectively. The solid and dotted lines indicate radiative and nonradiative processes, respectively. The dashed lines exemplify possible energy-transfer paths between the host and the Eu^{3+} ions and between the LMCT states and the $4f^6$ levels.

$\leq n \leq 400$, the decrease observed in the energy of the siliceous emitting centers as the radius of the nanodomains increases. The emission energies of the siliceous regions were obtained by an iterative least-squares curve-fitting procedure reported previously,[9] whereas the nanodomain sizes were calculated on the basis of small-angle X-ray scattering results.

IV. Conclusions

The energy-transfer processes and the measurements of the absolute emission quantum yields in two series of Eu^{3+}-based white light emitting hybrids whose host matrix is composed of siliceous nanodomais covalently bonded to polyether chains via urea cross-linkages were described. The energy-transfer mechanisms between the nanoscopic hosts and the cations arise from two different and independent processes: a charge-transfer band, resulting from the interaction between the Eu^{3+} and the first ligands, and energy transfer from the hybrid's backbone emitting centers (siloxane nanoregions and NH groups of the urea bridges). The energy-transfer processes and, therefore, the absolute emission quantum yields strongly depend on the Eu^{3+} local coordination. In the diureasils where the Eu^{3+} ions interact with the carbonyl-type oxygen atoms of the urea cross-links (located near the hybrid's emitting centers), the energy-transfer processes are active, with the corresponding decrease of the absolute emission quantum yields, relative to the undoped xerogel. On the contrary, when the Eu^{3+} ions are coordinated to the polymer chains, the distance between the hybrid's emitting centers and the metal ions is large enough to allow efficient energy transfer and thus the quantum yields are unchanged.

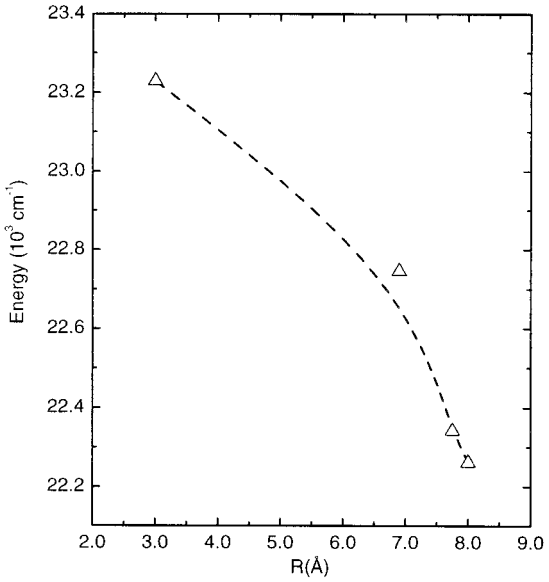

Figure 7. Variation of the fitted emission energy of the siliceous regions (excited at 375 nm) for $U(2000)_nEu(CF_3SO_3)_3$, $40 \leq n \leq 400$, with the respective nanodomain size. The line is drawn as a guide to the eyes.

The Eu^{3+}-based siloxane/POE nanohybrids are versatile and promising full-color emitters in which the overall emission characteristics are essentially determined by the tuning of the energy-transfer process between the different components of the nanohybrids, i.e., the siliceous nanodomains, the urea linkages, the POE chains, and the lanthanide centers. This tuning is easily achieved using both chemical—through the control of the molecular weight of the polyether segments and of the amount of Eu^{3+} incorporated into the nanoscopic matrix—and physical—variation of the excitation energy—approaches. Therefore, the most remarkable aspect of these nanocomposites is the possibility to tune the relative influence of the mentioned energy-transfer processes and to get nanostructured materials with potential use in silicon-compatible display technologies requiring fine control of an efficient white light emission. Furthermore, the incorporation of europium salts with ligands that sensitize the Eu^{3+} emission (efficient UV/vis conversion) may induce better performance concerning the nanohybrid's absolute quantum yields.

Acknowledgment. Financial support from FCT (Grants PRAXIS/P/CTM/13175/98 and BD/18404/98) and ICCTI (Portugal) and FAPESP and CAPES (Brazil) is gratefully acknowledged.

CM010311O